2008 IEEE International Conference on
Robotics and Automation
Pasadena, CA, USA, May 19-23, 2008

Design, Implementation and Test Results of a Robust Control Method for a Powered Ankle Foot Orthosis (AFO)

Alexander W. Boehler, Kevin W. Hollander, Thomas G. Sugar, Dosun Shin

***Abstract*— There are various methods to control a powered AFO. As different as they are in their approach each of them has certain advantages as well as difficulties. What is still needed is a robust control concept that meets the requirements for ankle gait assistance. A new, stiffness-control model has been developed that divides the stance phase of gait into five zones using either velocity or stiffness control for each zone. The design and implementation of this new control algorithm as well as some first test results are presented.**

I. INTRODUCTION

A great number of people will benefit from a powered ankle-foot orthosis. The applications vary from rehabilitation purposes using a treadmill to wearing an AFO in order to perform daily tasks in everyday life. One large group that will use a powered AFO are stroke survivors. Over 5.7 million people suffer from a stroke in the United States; this does not include patients of post-polio, multiple sclerosis, spinal cord injury or cerebral palsy [1],[2].

To make a powered AFO easily commercially available, one does not only need a reliable, safe and energy efficient design, but also simple and yet sophisticated controls for the device. Our initial systems have used simple position control of the motor with a predefined and adjustable gait pattern as the reference command.

In this paper, the advantages and drawbacks of the existing control concepts are shown. There is a need for more sophisticated control models. The design and implementation of one such advanced model will be presented. In the first section, a mathematical analysis will provide a basic understanding of the plant that is controlled as a background for the subsequent sections.

> *"There is a marked lack of published quantitative results on the performance of the active orthotic devices that have been developed. Considering this, one is left to wonder what real advantages of these complicated expensive systems really are."* [1]

Secondly, as stated in the above quote there is a lack of published data on powered AFO devices. Therefore, test results with different control concepts will be shown, which emphasize our control models.

Manuscript received September 14, 2007.

Alexander W. Boehler is with Arizona State University, Tempe, Arizona 85287-6106 alexander.boehler@asu.edu

Kevin W. Hollander is with Augspurger-Komm Engineering, Inc. Phoenix, Arizona 85040 kevin.hollander@asu.edu

Thomas G. Sugar is with Arizona State University, Polytechnic Campus, thomas.sugar@asu.edu

Dosun Shin is with Arizona State University, Tempe, Arizona 85287-6106 dosun.shin@asu.edu

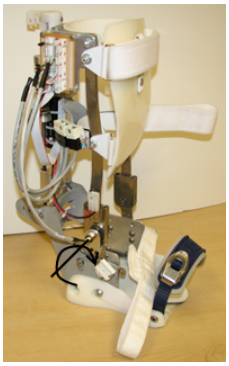

Fig. 1. Latest Version of the Robotic Tendon AFO

II. ROBOTIC TENDON

The Robotic Tendon consists of a DC motor in series with a custom threaded lead screw and spring. Fig. 1 shows the latest version of the Robotic Tendon AFO, which fits around a person's shoe for fast and easy attachment and detachment. With only 0.5kg for the actuator alone and 1.75kg for the system as a whole, it is a very light-weight design and is comfortable to wear. The currently used electronic structure consists of an Advantech 650MHz PC-104 computer with 512MB on board memory as a well as a Multifunctional I/O board from Sensoray Co. The current for the RE-30 motor is provided by a custom designed 160 Amp single motor controller developed by Robotics Group Inc. This controller also provides a measurement of motor current for true electrical power calculations. A digital incremental motor encoder is used to determine the position of the lead screw; an additional absolute angular encoder measures the position of the output side of the spring and ankle position. Force sensors attached to an insole that is inserted in the person's shoe are used to determine heel strike and toe contact states. Finally, to control the position of the nut on the lead screw a model for the amplifier and the DC motor is used, see Fig. 2.

A. Amplifier Model

Generally, a motor controller takes either an analog voltage or a pulse-width modulated signal as input and converts this signal into the correct armature voltage for the motor. The motor controller of the Robotic Tendon takes an analog voltage from 0 to 2.5 volts (forward) and 2.5 to 5 volts (reverse) as input and provides 24 volts as output for the motor. We therefore can use a gain K_c as a simple model for the motor amplifier.

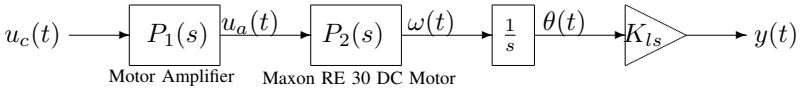

Fig. 2. Model of the Plant

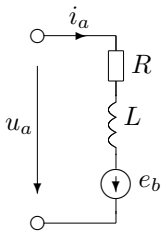

Fig. 3. Electric Diagram for a DC Motor

TABLE I
PARAMETERS FOR THE 2^{nd} GENERATION ROBOTIC TENDON ACTUATOR

Parameter	Value	Unit
K_c	9.6	1
K_{ls}	1.27	mm/revolution
K_t	25.9	mNm/A
K_e	0.00271	V/rpm
R_a	0.611	Ω
L_a	0.12	mH
J	681	gcm^2
b	0.0065	kgm^2/s

$$P_1(s) = \frac{U_a(s)}{U_c(s)} = K_c \tag{1}$$

Herein, $U_c(s)$ denotes the control voltage sent to the amplifier and $U_a(s)$ denotes the armature voltage of the motor, given from the amplifier, see also Fig. 2.

B. DC Motor Model

Fig. 3 shows the electric diagram for a standard DC motor. Generally, a DC motor has a resistance R_a due to the wiring as well as an inductance L_a due to the rotor. The rotation of the rotor due to the electromagnetic force at the same time causes the induction of a voltage which is called *back emf* (back electromotive force), e_b in the diagram. Kirchhoff's voltage law for Fig. 3 yields

$$L_a \frac{di_a}{dt} + R_a i_a + e_b = u_a \quad . \tag{2}$$

Applying Lorentz's and Faraday's laws yields the following equations for the torque T and back emf e_b, whereas $K_t = lBr_1$, $K_e = r_2Bl$ and $[K_t] = Nm/A$, $[K_e] = V/rpm$. These constants can usually be found in the specification sheet of a motor. The vectors are considered as being normal to each other to simplify the equations [3].

$$T = K_t i_a \tag{3a}$$

$$e_b = K_e \omega \tag{3b}$$

Newton's second law of motion for the movement of the load gives us the dynamics of the load with J being the overall inertia seen by the motor.

$$J\dot{\omega} + b\omega = T \tag{4}$$

After taking the Laplace Transforms of the equations and substituting them into each other, the following transfer function from the motor voltage u_a to the shaft velocity ω can be derived.

$$\begin{aligned} P_2(s) &= \frac{\Omega(s)}{U_a(s)} = \\ &= \frac{K_t}{L_a J s^2 + (R_a J + L_a b)s + R_a b + K_e K_t} \end{aligned} \tag{5}$$

Given the parameter values, the transfer function can be derived from the control voltage u_c to the nut position y. K_{ls} is dependent on the pitch of the lead screw and has the unit $mm/revolution$.

$$\frac{Y(s)}{U_c(s)} = \frac{K_c K_t K_{ls}}{s\left(L_a J s^2 + (R_a J + L_a b)s + R_a b + K_e K_t\right)} \tag{6}$$

Given the actual values for each of the parameters one can use this transfer function to design a controller for the system. For the 2^{nd} generation Robotic Tendon actuator the parameters shown in Table I were found.

Since the terminal inductance L_a is very small, the following approximate transfer function from U_c to Y can be used to describe the system.

$$T_{u_c y} \approx \frac{K_c K_t K_{ls}}{s\left(R_a J s + R_a b + K_e K_t\right)} \cdot \frac{2/\Delta - s}{2/\Delta + s} \tag{7}$$

Note, an additional term was added to the transfer function. This term models the time delay that one will find in any real world system. This time delay results from signals being processed and the magnetic fields being generated until the motor finally reacts. The time delay is modeled using the Padé[1] approximation and the parameter Δ was found to be 0.008.

[1]The Padé approximation uses the following linear expression to approximate the non-linear time delay in the s-domain $e^{-as} \approx \frac{1-as/2}{1+as/2}$.

C. Short Analysis of the Model

From (7) it can be seen that the plant has poles at

$$s = 0, \quad -\frac{R_a b + K_e K_t}{R_a J}, \quad -\frac{2}{\Delta}$$

and that the system will be *unstable* due to the pole at the origin. The open-loop step responses of the simulated model with the parameter set provided in Table I and the real system can be seen in Fig. 4.

Using basic root locus theory, one can find the possible controller structures that will provide stability for this system. Already a proportional controller can stabilize the system; however, for improved performance one may want to add a differential and/or integral term. Also, the plant already has an integral part included, which gives the closed-loop system the ability to follow step reference commands. An I-controller will *never* be able to stabilize the system.

III. EXISTING CONTROL MODELS

In this section basic control methods are presented and analyzed. Fig. 5 shows a schematic of the mechanical linkage for a Robotic Tendon.

A. Lever Control

In this control law, the actual lever position l_a is measured, for instance, with a linear potentiometer and then subtracted from a given reference command r. Equation (8) expresses the described control law using a PD - Controller with u_c being the control voltage sent to the motor amplifier.

$$u_c = K_p \left(r - l_a\right) + K_d \left(\dot{r} - \dot{l}_a\right) \tag{8}$$

This simple control law can easily be implemented and tested. However, since the controller is controlling the output-side of the spring, it will force the user to follow the pattern given by r. The user has no other choice than move in the same pattern as the robot.

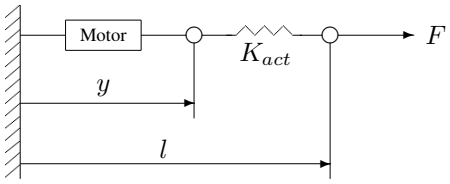

Fig. 5. Model of the Robotic Tendon

B. Nut Control

A second possibility is to control the position of the nut y, which is the backside of the spring. The actual nut position y_a can easily be measured with a motor encoder and then subtracted from a given reference command r. Equation (9) expresses the described control law using a PD - controller.

$$u_c = K_p \left(r - y_a\right) + K_d \left(\dot{r} - \dot{y}_a\right) \tag{9}$$

Because we are now controlling the input side of the spring, this means that the spring can act as a safety device and can compensate for small errors of the human or the robot, which highly increases wearer comfort.

Therefore, nut control is a very robust and safe control method and good test results in terms of power output and input are achieved with this method [4],[5]. Fig. 6 shows the kinematics for one gait cycle. It can be seen that the controller does its job very well and although the lever is open-loop controlled, the resulting path is still close to the curve found in theoretical texts for ankle gait kinematics [6]. Fig. 7 shows the measured mechanical input (nut) and output (lever) power for one gait cycle. Note that the test was performed with an able-bodied subject with a body weight of 65kg and a walking speed of about 1m/s. The robot is designed for 50% gait assistance. It can be seen that power output is greater than power input because the spring stores and releases energy. The ratio is $P_{out}/P_{in} \approx 2.12$. A reduction of required motor power significantly reduces required motor size and weight.

However, limitations are reached as soon as optimization of the controller for certain stages during gait is desired. Other limitations include changing the reference command,

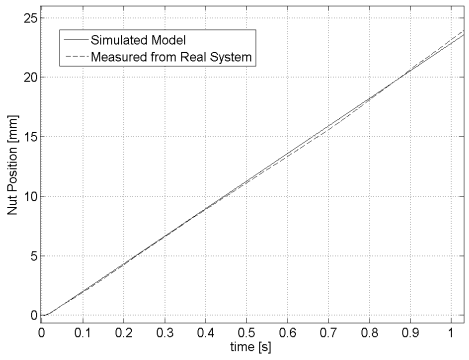

Fig. 4. Step Responses for Simulated Model and Real System

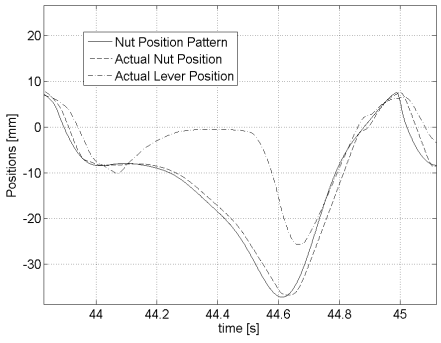

Fig. 6. Kinematics of One Gait Cycle

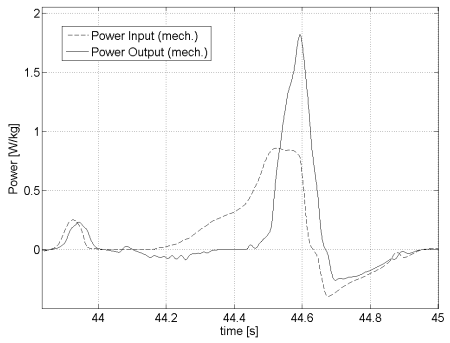

Fig. 7. Mechanical Power Input and Output of One Gait Cycle

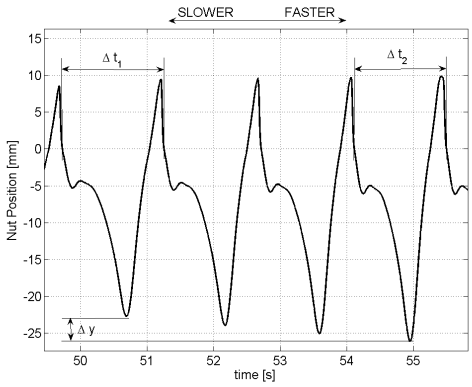

Fig. 8. Nut Profile adjusted in Time and Amplitude

which essentially is a gait pattern, to adjust itself for different walking speeds or different activities such as walking versus stair climbing.

The first approach to this problem is to adjust the nut profile in its duration in time as described in [4], [5]. One approach to adjust the profile is by fitting a polynomial curve through nut profiles with different durations and then find a mathematical correlation between them.

Generally, it can be said that the amplitudes of plantarflexion and dorsiflexion become smaller with lower speeds. In a second approach, the nut profile is adjusted not only in its duration in time but also in its amplitude as shown in Fig. 8. Note that with increasing speed the pattern shrinks in time (i.e. $\Delta t_2 \leq \Delta t_1$) while its amplitude increases (Δy). This method works very well, however, a few difficulties remain.

Firstly, the controller cannot be optimized for different stages during gait or for different situations. One can easily imagine that, as soon as a person is walking over uneven ground instead of on a treadmill, the whole profile will change as well. Secondly, this method will always be one gait cycle too late, since it uses the stride time of the last gait cycle to adjust the current gait cycle.

IV. THE ROBUST CONTROL CONCEPT

The discussion of different control laws in the previous section has shown that very good results with the existing control models, in particular with nut control, were achieved but that we desire to eliminate some of their disadvantages. The theoretical foundation for a very promising new method has been developed by Sugar and Hollander [7], [8]. Their approach is a mixture between stiffness control and velocity control. They suggest to split the stance phase of gait into five distinct zones and then set the stiffness or velocity for a certain phase.

A. Equilibrium Controlled Stiffness

In the diagram of Fig. 5, the external force can be determined.

$$F = -K_{act} \cdot (l - y - d) \tag{10}$$

F is the force applied at the end of the spring whereas d denotes the free length of the spring. Shown earlier by Sugar [7], one can develop a relationship for the motor position that allows the device to exhibit the behavior of any desired value of stiffness. The following equation describes this relationship.

$$F = -K_{des} \cdot (l - l_0) + f_{des} \quad . \tag{11}$$

Herein, K_{des} denotes the desired stiffness; l_0 is the virtual home position and f_{des} denotes the simulated preload. This can be substituted into (10). Solving for the motor position y yields the required control law.

$$y = \left(1 - \frac{K_{des}}{K_{act}}\right) \cdot l + \frac{K_{des}}{K_{act}} \cdot l_0 + \frac{f_{des}}{K_{act}} - d \tag{12}$$

This rather simple control law achieves stiffness control for one link. To show how powerful this control law is, consider two special cases for the desired stiffness K_{des}. For simplicity we will assume a zero length spring and the home position for both cases is the same. Therefore, l_0, f_{des} and d are all equal to zero.

Case 1: $K_{des} = 0$. Equation (12) then becomes

$$y = l \quad . \tag{13}$$

This means that the motor will behave as if the spring was infinitely soft and will just follow whatever the lever (in the case of the robotic tendon this is the user) does. Hence, this control law could be used to obtain measurements for the ankle angle profile for different persons.

Case 2: $K_{des} = K_{act}$. Equation (12) then becomes

$$y = 0 \quad . \tag{14}$$

When the desired stiffness is equal to the physical spring stiffness this means that the motor will hold its position.

B. Combination of Velocity and Stiffness Control

In [8], Hollander suggests to split up the stance phase of gait into five distinct zones, see Fig. 9, whereas each zone will be governed by a certain control law, either velocity control or stiffness control. In this figure the circled numbers are zones that can be described by linear stiffness values while the other two zones, which are represented by

square numbers, are described by constant velocity. While the desired stiffness can be calculated using ankle gait data, for instance from [6], the actual stiffness of the actuator needs to be chosen by the designer and remains fixed. In this method, the actual stiffness is designed to match the desired stiffness in zone 5.

For *zone 1*, which starts at heel strike, the author suggests to use velocity control to keep the motor velocity constant and at a level proportional to the speed of the previous swing phase.

Zone 2 starts when the ankle angular velocity, $\dot{\theta}$, crosses through zero. For this zone it is suggested to maintain a constant stiffness which is 1.35 times the actual spring stiffness.

For, *zone 3*, which starts at flat foot and occupies most of the loading phase, again a constant stiffness should be applied which is 3 times the actual stiffness of the spring.

Zone 4 starts when the heel lifts off the ground. It is suggested to maintain a constant velocity during this zone that is equal to the motor velocity in the previous zone.

Zone 5 starts as the body can no longer resist the energy that was stored in the spring and therefore the energy is released which propels the body forward. For this phase it is important for the motor to just "hold position", hence allowing the energy to be released. The end of this zone is when all the stored energy of the spring has been released and the swing phase begins.

What is fascinating and promising about this approach is, that the motor control action follows a simple *stretch - hold - release* pattern. In the method described in section III-B, a fixed pattern is fed to the motor. This is based on experimental data which represents an average gait cycle. However, every person has their own way of walking as well as their own walking speed and although the spring can compensate for small errors, the system is not as flexible. Using this new method, the controller eliminates the time dependence and allows dynamic adjustment to the walking pattern by only detecting the transitions between each zone.

C. Implementation

As was briefly mentioned, a digital incremental encoder is used at the motor to control its position. Additionally an absolute angular encoder for measuring the ankle angle, and subsequently the lever position, the spring deflection and force, is used as well to zero the robot. In order to detect the transitions between the zones, a heel and toe switch is needed. The heel switch is used to detect heel strike, whereas the toe switch is used to detect flat foot.

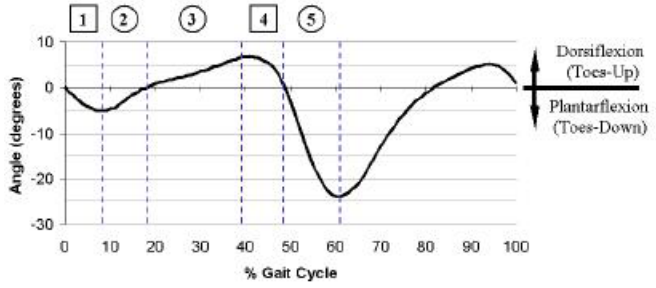

Fig. 9. Ankle Angle Divided Into Zones for One Gait Cycle [8]

The control structure fits perfectly into a (finite) state machine. Fig. 10 shows the state machine that was implemented with MATLAB stateflow. The arrows with a full black circle at their tail denote default states that are entered when there is ambiguity between two or more states.

Note that six other states have been added to the ones discussed in section IV-B. Firstly, when the system is turned on, variables are initialized and the controller waits for a user command, which in this case is the activation of the hand switch, in order to begin zeroing. Upon completion of the zeroing procedure, the system goes into a safe mode where the motor maintains zero stiffness, so the person can walk with the robot with zero motor assistance. Another press of the hand switch brings the system into a ready state where it waits for the heel switch in order to begin powered gait assistance. The goal during swing phase is rather simple. The robot brings the foot up quickly so that the person does not drag their toes over the ground. Therefore, it was decided to maintain a constant velocity through this phase (6) until the ankle angle reaches a certain amount of dorsiflexion. Lastly, the motor will again hold position and wait until the next heel strike occurs. This last phase is labeled 7 in Fig. 10.

D. Test Results

The robust control method described previously was tested on an able bodied subject with a body weight of 65kg, walking at a speed of 1.25m/s. The robot is designed for 50% assistance. Fig. 11 shows the kinematics as well as the phases of one gait cycle. Note that the phase numbers are assigned from 11 to 17 for the seven phases for a gait cycle in Fig. 10. It can be seen that the controller switches through the phases as planned in section IV-B and section IV-C and that the resulting kinematics match up well with the theory. During phase one the foot is brought to the ground with a given velocity. Phase three shows the energy storage in the spring where the user and motor drive in opposite directions due to setting the desired stiffness equal to three times the actual spring stiffness. The spring deflection is indicated by the shaded area between the nut and lever curve. During phase five the motor holds position and the stored energy is released. Results show the ratio of power input to power output has an amplification factor of about $\max(P_{out})/\max(P_{in}) \approx 1.89$.

V. CONCLUSION

The test results using the new stiffness based controller are encouraging. Firstly, since clear and simply detectable transition signals were used, the controller was able to switch through the states continuously without getting locked into one state. Secondly, the motor and lever curves that have been obtained during the test are similar to the ones that are obtained through simulation in [8], which verifies the models. Thirdly, no predefined nut pattern was used to obtain the

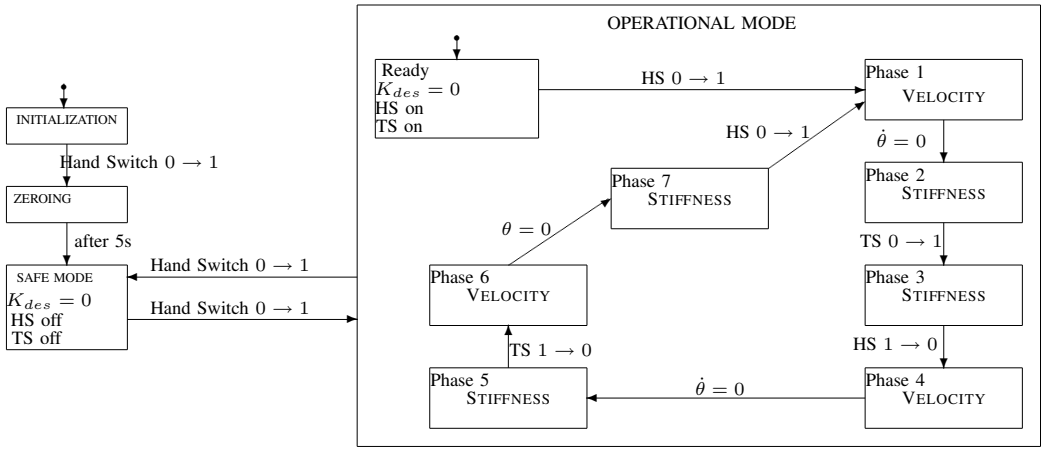

Fig. 10. Implemented State Machine, HS ... Heel Switch, TS ... Toe Switch

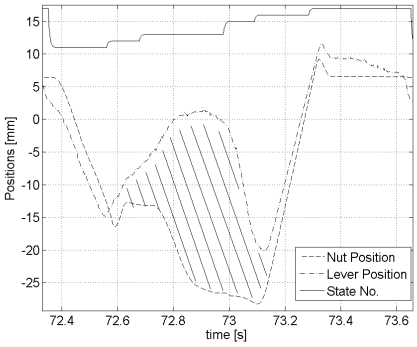

Fig. 11. Kinematics

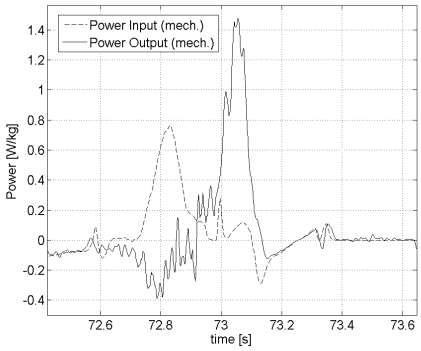

Fig. 12. Mechanical Power Input and Output of One Gait Cycle

curves shown in section IV-D. Still the motor path matches the previously used pattern well. At the same time, the lever displacement, which is open-loop controlled, matches a normal person's gait. The robot is interacting with the user rather than forcing the user into its pattern.

Therefore, these results encourage further research and testing. These tests show that we can achieve similar power in to power out ratios and similar motor paths with this new control law. The first test of this control structure was an important step and brings the overall project closer to the goal of creating an intuitive and robust control methodology for a robotic tendon actuator.

VI. ACKNOWLEDGMENTS

The authors gratefully acknowledge the support of the National Institute of Health (NIH), as well as the invaluable contributions of Robotics Group Co. and Arise Prosthetics.

REFERENCES

[1] Dollar, A. M. and Herr, H. "Active Orthoses for the Lower-Limbs: Challenges and State of the Art", *2007 IEEE* 10^{th} *International Conference on Rehabilitation Robotics (ICORR)*

[2] American Heart Association (2007). [Online]. Available: http://www.americanheart.org

[3] A. A. Rodriguez, "Analysis and Design of Feedback Control Systems", Textbook, pp. 180-182, 2003.

[4] J. K. Hitt, M. A. Oymagil, T. G. Sugar, K. W. Hollander, A. W. Boehler, J. Fleeger, 2007. "Dynamically Controlled Ankle Foot Orthosis (DCO) With Regenerative Kinetics: Incrementally Attaining User Portability", *2007 IEEE Conference on Robotics and Automation (ICRA)*

[5] M. A. Oymagil, J. K. Hitt, T. G. Sugar, 2007. "Control of a Regenerative Braking Powered Ankle Foot Orthosis", *2007 IEEE* 10^{th} *International Conference on Rehabilitation Robotics (ICORR)*

[6] W. M. Whittle, "Gait Analysis: An Introduction", 2nd ed. Butterworth-Heineman Oxford.

[7] T. G. Sugar, 2001. "A Novel Selective Compliant Actuator" *Journal of Mechatronics, Volume 12, Number 9, November 2002.*

[8] K. W. Hollander and T. G. Sugar 2007. "A Robust Control Concept for Robotic Ankle Gait Assistance", *2007 IEEE* 10^{th} *International Conference on Rehabilitation Robotics (ICORR)*

[9] S. R. Lazarevic and S. M. Jaukovic, "Logic Control of Partial Active Orthoses via Real-Time Computing System," *Proceedings of the International Symposium on External Control of Human Extremities*, pp. 247-257, 1975.

[10] D. P. Ferris, J. M. Czerniecki, B. Hannaford, "An Ankle-Foot Orthosis Powered by Artificial Muscles," *Journal of Applied Biomechanics*, vol. 21, pp. 189-197, 2005.

[11] G. S. Sawicki, K. E. Gordon, D. P. Ferris, "Powered Lower Limb Orthoses: Applications in Motor Adaptation and Rehabilitation", *Proceedings of the 2005 IEEE International Conference on Rehabilitation Robotics (ICORR)*, pp. 206-211, 2005.

[12] National Stroke Association (2007). [Online]. Available: http://www.stroke.org